



## 저작자표시-비영리-변경금지 2.0 대한민국

이용자는 아래의 조건을 따르는 경우에 한하여 자유롭게

- 이 저작물을 복제, 배포, 전송, 전시, 공연 및 방송할 수 있습니다.

다음과 같은 조건을 따라야 합니다:



저작자표시. 귀하는 원저작자를 표시하여야 합니다.



비영리. 귀하는 이 저작물을 영리 목적으로 이용할 수 없습니다.



변경금지. 귀하는 이 저작물을 개작, 변형 또는 가공할 수 없습니다.

- 귀하는, 이 저작물의 재이용이나 배포의 경우, 이 저작물에 적용된 이용허락조건을 명확하게 나타내어야 합니다.
- 저작권자로부터 별도의 허가를 받으면 이러한 조건들은 적용되지 않습니다.

저작권법에 따른 이용자의 권리는 위의 내용에 의하여 영향을 받지 않습니다.

이것은 [이용허락규약\(Legal Code\)](#)을 이해하기 쉽게 요약한 것입니다.

[Disclaimer](#)

Thesis for the Degree of Master of Engineering

Fabrication of Long-Period Fiber  
Gratings on Double-Clad Fiber using  
CO<sub>2</sub> Laser and their Responses to  
Various Physical Parameters



by

Jonatan Martino Windi Saputro

Department of Industry 4.0 Convergence Bionics Engineering

The Graduate School

Pukyong National University

February, 2023

Fabrication of Long-Period Fiber  
Gratings on Double-Clad Fiber using  
CO<sub>2</sub> Laser and their Responses to  
Various Physical Parameters  
(CO<sub>2</sub> 레이저를 이용한 이중-클래딩  
광섬유 상 장주기 광섬유 격자의  
제작 및 제작된 격자의 다양한  
물리적 변수에 대한 반응)

Advisor: Prof. Yong Wook Lee

by

Jonatan Martino Windi Saputro

A thesis submitted in partial fulfillment of the requirements  
for the degree of  
Master of Engineering  
in Department of Industry 4.0 Convergence Bionics Engineering,  
The Graduate School,  
Pukyong National University

February, 2023

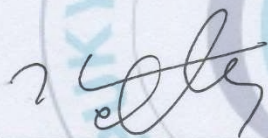
Fabrication of Long-Period Fiber Gratings on Double-Clad Fiber  
using CO<sub>2</sub> Laser and their Responses to Various Physical  
Parameters

A thesis

by

Jonatan Martino Windi Saputro

Approved by:



(Chairman) Prof. Hyun Wook Kang



(Member) Prof. Joong Ho Shin



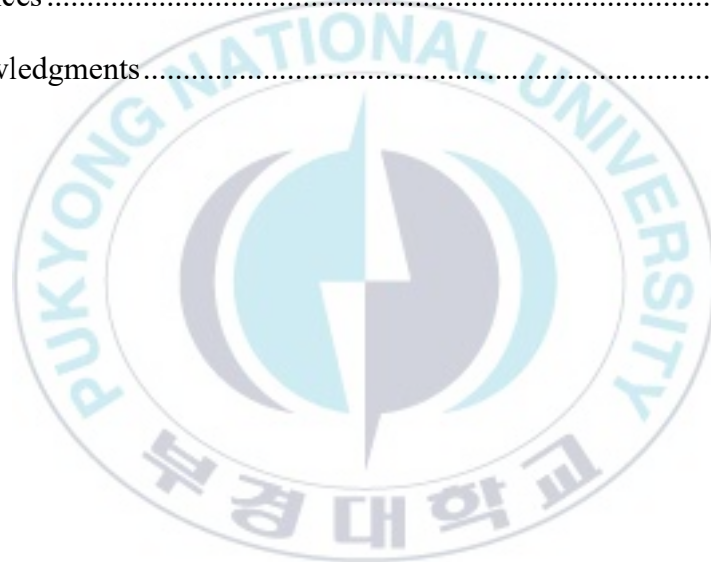
(Member) Prof. Yong Wook Lee

February 17, 2023

## Table of Contents

Table of Contents .....	i
List of Figures .....	iii
I. Introduction.....	1
II. Theoretical Basis .....	4
2.1 Fiber Optics.....	4
2.1.1 Optical Fiber Waveguide.....	4
2.1.2 Single-Mode Fiber .....	8
2.1.3 Double-Clad Fiber .....	10
2.2 Long-Period Fiber Grating.....	11
2.3 LPFG Fabrication with CO <sub>2</sub> Laser.....	14
III. LPFG Fabrication.....	18
3.1 Fabrication.....	18
3.2 Transmission Characteristics .....	20
IV. Experimental Preparation and Measurement Results .....	22
4.1 Experiment Setup .....	22
4.1.1 Bending Measurement .....	22
4.1.2 Strain Measurement .....	24
4.1.3 Torsion Measurement .....	24

4.1.4 Temperature Measurement .....	25
4.2 Measurement Results .....	27
4.2.1 Bending Measurement Results .....	27
4.2.2 Strain Measurement Results .....	29
4.2.3 Torsion Measurement Results .....	31
4.2.4 Temperature Measurement Results.....	34
V. Conclusion.....	37
References .....	39
Acknowledgments.....	51





## List of Figures

<b>Figure 1.</b> Three general types of fibers.....	13
<b>Figure 2.</b> Illustration of disturbance in core mode propagation LPG.....	17
<b>Figure 3.</b> Refractive index profile (top) of a double-layered fiber (DCF) and schematic cross-sectional structure (bottom) .....	18
<b>Figure 4.</b> Schematic of the working principle of LPG. ....	19
<b>Figure 5.</b> Schematic of a typical LPFG fabrication system based on a point-to-point technique using a CO <sub>2</sub> laser. ....	22
<b>Figure 6.</b> Schematic diagram for fabrication of long-period fiber gratings on double-clad fiber using CO <sub>2</sub> laser.....	26
<b>Figure 7.</b> (a) Schematic diagram of core and cladding structure of DCF-LPFG and (b) optical microscope image of fabricated DCF-LPFG .....	19
<b>Figure 8.</b> Transmission spectrum of fabricated DCF-LPFG measured at room temperature without any applied strain or torsion.....	28
<b>Figure 9.</b> Schematic diagram of experimental setup designed to investigate bending responses of fabricated sensor head (DCF-LPFG).....	30
<b>Figure 10.</b> Schematic diagram of experimental setup designed to investigate strain responses of fabricated sensor head (DCF-LPFG).....	31
<b>Figure 11.</b> Schematic diagram of experimental setup designed to investigate torsion responses of fabricated sensor head (DCF-LPFG).....	32
<b>Figure 12.</b> Schematic diagram of experimental setup designed to investigate temperature responses of fabricated sensor head (DCF-LPFG).....	33
<b>Figure 13.</b> Spectral variations of sensor indicators (a) Dip A and (b) Dip B, induced by applied bending of 0.0 to 1.22 m <sup>-1</sup> . The insets of (a) and (b) show the bend-induced wavelength shifts of Dip A and Dip B, respectively. ....	36
<b>Figure 14.</b> Spectral variations of sensor indicators (a) Dip A and (b) Dip B, induced by applied strain of 0 to 2000 µε. The insets of (a) and (b) show the strain-induced	

wavelength shifts of Dip A and Dip B, respectively.....	37
<b>Figure 15.</b> Spectral variations of sensor indicators (a) Dip A and (b) Dip B, induced by applied twist of $-180^\circ$ to $180^\circ$ . The insets of (a) and (b) show the torsion-induced wavelength shifts of Dip A and Dip B, respectively.....	40
<b>Figure 16.</b> Spectral variations of sensor indicators (a) Dip A and (b) Dip B, induced by applied temperature of 25 to 100 $^\circ\text{C}$ . The insets of (a) and (b) show the thermal-induced.....	43





# CO<sub>2</sub> 레이저를 이용한 이중-클래딩 광섬유 상 장주기 광섬유 격자의 제작 및 제작된 격자의 다양한 물리적 변수에 대한 반응

Jonatan Martino Windi Saputro

부경대학교 대학원 4차산업융합바이오닉스공학과

## 요약

우리는 다양한 물리적 매개변수들을 측정하기 위해 이중 클래드 광섬유(double-clad fiber : 이하 DCF)에 10.6  $\mu\text{m}$ 의 장주기 격자(long-period fiber grating: 이하 LPFG)를 각인한 광섬유 센서를 제안한다. DCF에 각인된 LPFG를 앞으로 DCF-LPFG라 언급하며, 다른 cladding-mode로 인한 다양한 공진 딥(resonance dip)들이 존재하며 그들 중 2개의 공진 딥을 센서의 지시자로 선택하였다. 측정된 물리적 파라미터는 벤딩, 변형, 비틀림 및 온도이다. 측정된 센서 지표의 굽힘 민감도는 굽힘 곡률 범위 0.0 ~ 1.22  $\text{m}^{-1}$ 에서 약 -4.422 및 -21.88  $\text{nm}/\text{m}^{-1}$ 로 측정되었다. 측정된 센서 지시딥의 당김에 대한 민감도는 0 ~ 2000  $\mu\text{m}$  범위에서 약 -0.171  $\text{pm}/\mu\text{m}$  및 5.029  $\text{pm}/\mu\text{m}$ 로 나타났다. 비틀림에 대한 민감도는  $-180^\circ \sim +180^\circ$  범위 내에서 114.80 and 56.04  $\text{pm}/(\text{rad}/\text{m})$ 의 민감도를 나타냈으며,  $25^\circ\text{C} \sim 100^\circ\text{C}$  온도 범위에서는  $\sim 67.70$  and  $\sim 67.44$   $\text{pm}/^\circ\text{C}$ 의 민감도로 측정되었다. 네개의 물리적 매개변수를 측정한 결과 DCF-LPFG 응답은 양호한 성능을 보였으며 민감하고 둔감한 응답을 보였다. 이 센서 헤드는 잠재적으로 향후 작업을 위해 두 개 이상의 물리적 파라미터를 동시에 측정할 것이다. 제안된 DCF-LPFG는 다양한 산업 현장에서 비용적인 이점이 충분한 센서 헤드으로써 건물 구조의 안전성 진단에 유용하게 사용 될 것이라 기대한다.

# **Fabrication of Long-Period Fiber Gratings on Double-Clad Fiber using CO<sub>2</sub> Laser and their Responses to Various Physical Parameters**

Jonatan Martino Windi Saputro

Department of Industry 4.0 Convergence Bionics Engineering

Graduate School of Engineering

Pukyong National University

## **Abstract**

Here we report an optical fiber sensor capable of performing various physical parameters measurements using a long-period fiber grating (LPFG) inscribed on double-clad fiber (DCF) with a 10.6  $\mu\text{m}$  CO<sub>2</sub> laser. The LPFG inscribed on DCF, referred to as DCF-LPFG, exhibited multiple resonance dips with different cladding-mode orders, and two of them were selected as sensor indicators. The physical parameters measured are bending, strain, torsion, and temperature. The measured bending sensitivities of the sensor indicators were approximately -4.422 and -21.88  $\text{nm}/\text{m}^{-1}$  in a bending curvature range of 0.0 to 1.22  $\text{m}^{-1}$ . The measured strain sensitivities of the sensor indicators were approximately -0.171 and 5.029  $\text{pm}/\mu\epsilon$  in a strain range of 0 to 2000  $\mu\epsilon$ . The measured torsion sensitivities of the sensor

indicators were approximately 114.80 and 56.04 pm/(rad/m) in a twist angle range of  $-180^{\circ}$  to  $180^{\circ}$ , and their temperature sensitivities were measured as  $\sim 67.70$  and  $\sim 67.44$  pm/ $^{\circ}\text{C}$  in a temperature range of 25 to 100  $^{\circ}\text{C}$ . The DCF-LPFG response from the measurement of four physical parameters showed good performance and shows a sensitive and insensitive response. This sensor head potentially simultaneously measures two or more physical parameters for future work. The proposed DCF-LPFG is expected to be beneficial as a compactly embedded and electrically passive cost-effective sensor head for structural health monitoring in various industrial trial applications.

Keywords: Long-period fiber grating, double-clad fiber, Optical fiber sensor, bending, strain, torsion, temperature.

## I. Introduction

To date, optical fiber-based devices have been widely used in various fields, including optical sensing and communication. Particularly in the field of optical communication networks, the operation of optical fiber-based devices includes wavelength filtering, optical switching, optical sensors, and signal processing <sup>1-5</sup>. Among other things, fiber optic sensors have shown unique potential in applications in various fields, such as structural health and environmental monitoring due to their fast response, durability, waterproof properties, corrosion resistance, and immunity to electromagnetic interference <sup>6,7</sup>.

Fiber grating is one of the most popular fiber optic devices and has been widely used in the field of optical communication and fiber optic sensing. From the research that has been done so far, two types of fiber gratings have been developed. According to the index modulation period, fiber gratings can be categorized into two types, namely into Bragg fiber gratings (FBGs) with optical wavelength periodicity and long-period fiber gratings (LPFGs) with a periodicity of several hundred wavelengths <sup>8,9</sup>. LPFG has been applied for many uses including erbium-doped fiber amplifiers for flattening the gain spectrum and in monitoring the transmitted power level in optical fiber <sup>10,11</sup>.

When compared to FBG, in use of LPFG exhibits a resonant attenuation band in its transmission spectrum, which is much wider and more adjustable than FBG. Because the effective refractive index (RI) of the fiber core and cladding and grating period affect the resonance wavelength, and for its level of sensitivity, LPFG is more sensitive than FBG to various measurements such as temperature <sup>12</sup>, torque <sup>13</sup>, bending <sup>14</sup>, and pressure <sup>15</sup>. Due to the codirectional mode coupling, the LPFG is also sensitive to the surrounding RI medium <sup>16</sup> and can be used to measure external RI changes.

LPFG fabrication by traditional or older methods is made by exposing photosensitive optical fibers to ultraviolet (UV) light transversely either through a point-to-point or amplitude mask to create a periodic refractive index change inside of an optical fiber. Recently, with another fabrication method, LPFG has been made by various other techniques namely carbon dioxide (CO<sub>2</sub>) laser beam exposure. The physical process by which a change in refractive index is induced in the optical fiber during exposure to CO<sub>2</sub> laser beam gives this LPFG unique properties compared to other traditional LPFGs fabricated by exposure to UV light <sup>17,18</sup>.

In this paper, we experimentally demonstrated the sensor and its response to various physical parameters by incorporating an LPFG inscribed

on DCF, hereafter referred to as DCF-LPFG with a high-frequency CO<sub>2</sub> laser, as a sensor head. To make a DCF-LPFG as a sensor head, we splice the DCF segment with a single mode fiber (SMF) segment before the grating fabrication. The fabricated sensor head showed two resonance dips with different cladding-mode orders due to codirectional mode coupling in the grating region, and two attenuation dips whose resonance wavelengths were  $\lambda_A = \sim 1508.62$  nm and  $\lambda_B = \sim 1551.88$  nm were selected as sensor indicators denoted by Dip A and Dip B, respectively. With these sensor indicators, bending, strain, torsion, and temperature responses were investigated in a bending curvature range of 0.00 -1.22 m<sup>-1</sup>, strain range of 0-2000 $\mu\epsilon$ , a twist angle range of -180° to 180° and a temperature range of 25 to 100 °C, respectively.

In the following section, we explain the fabrication process of the sensor head and the principle of operation of our sensor. Then, we will provide experimental results on the bending, strain, torsion, and temperature responses of the fabricated sensor head. After that, a summary and conclusions are presented at the end of the section.



## II. Theoretical Basis

### 2.1 Fiber Optics

#### 2.1.1 Optical Fiber Waveguide

Basically the underlying principle of optical fiber behavior is Snell's law:  $n_1 \sin(\theta_1) = n_2 \sin(\theta_2)$ , where the incident light or wave strikes or passes through the interface between media of refractive index  $n_1$  and  $n_2$ , respectively. With an incident angle of  $\theta_1$  and refractive angle of  $\theta_2$  concerning the normal to the interface.

The propagation pattern of a ray optic will alter at the interface of media with different RI is a prediction from Snell's law. The incident angle will be bigger than that of the refractive angle, if  $n_1 < n_2$ , and vice versa, with the expression of the refractive angle, deduced from Snell's law:  $\theta_2 = \arcsin(n_1/n_2 \sin(\theta_1))$ . Since the upper bound of the sine function is 1, it is possible to create situations where real number solutions are not allowed under the condition  $n_1 > n_2$ . The angle of incidence at which Snell's law ceases to apply, under conditions  $n_1 > n_2$ , is called the critical angle, where  $\theta_{\text{critical}} = \theta_{\text{incident}} = \arcsin(n_2/n_1)$ . For an optical ray whose critical angle is smaller than the incident angle, the ray will not pass through the interface and all its

transmission power and information will be retained and reflected into the incident medium. Such an optical phenomenon is called total internal reflection (TIR). TIR guarantees the wave amplitude and phase integrity of the incident wave, sustaining its propagation in the incident medium without power. The application of TIR underlies the invention of fiber optics, in which silica or plastic fibers serve as dielectric waveguides and limit the transmission of optical waves along the longitudinal axis of the fiber. Optical fiber has a more flexible and deformable structure. Optical waves propagating along optical fiber suffer from immune to electromagnetic interference and low loss of attenuation over long distances, making them perfect for telecommunications, power transmission, imaging and spectroscopy, fiber-optic sensors, and many, more.

An optical fiber consists of two general layers: the fiber core and the cladding which is the cylindrical transverse structure of the optical fiber. The total reflection of transmissive optical waves in optical fiber occurs at the boundary between the core and cladding, with the RI of the fiber cladding slightly lower than that of the core. Because especially for step-index optical fibers where the RI is homogeneous in the core or cladding, the core is usually made of  $\text{SiO}_2$  material doped with Ge and/or B materials, while the material

forming the cladding is made of pure fused silica material. The main causes of the difference in RI between the fiber core and cladding are the dopants within the fiber core and the residual stresses that accumulate during the fiber fabrication process. The value of the difference can be as small as 0.005 to 0.01, or 0.35% to 0.7% of the core RI<sup>19</sup>. From the analysis obtained from the waveguide and the deduction from Maxwell's equations, only discrete and finite optical wave spatial modes are allowed to propagate along the optical fiber. Therefore, the category of optical fiber is generally only divided into three types: single mode fiber (SMF), multimode fiber (MMF), and stepped index fiber. They are illustrated in Fig. 1.

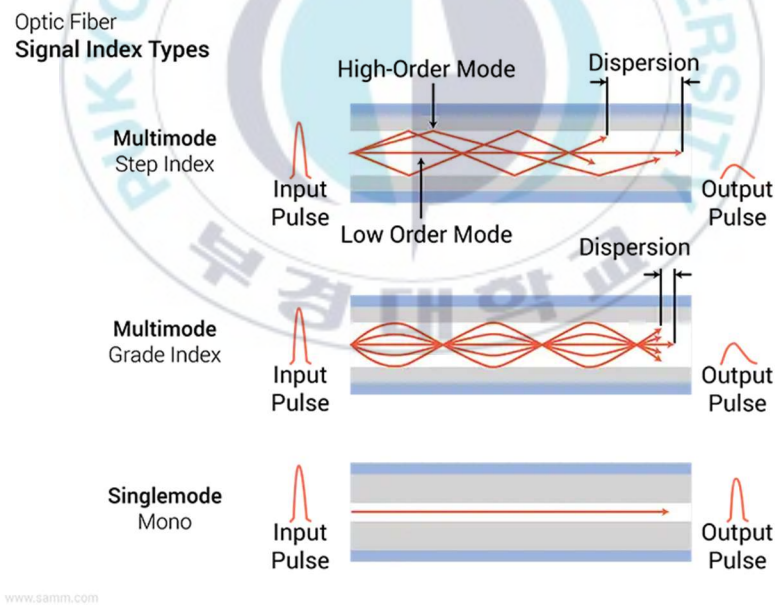


Figure 1: Three general types of fibers.

As we see in the figure, the top: is multimode fiber, whose core radius is large enough to accommodate multiple modes of optical waves. Middle: multimode graded-index fiber, whose RI of core varies along the radius. Bottom: single mode fiber, whose radius is much smaller than that of its core, resulting in only one mode allowed in transmission. MMF along with graded-index multimode fiber can support the propagation of multiple modes within the core. However, mode dispersion may occur because the different modes interfere with each other's transmission. Waveguide analysis from MMF states that it cannot withstand pulse dispersion and signal distortion. In contrast, SMF shows the advantage of having lower dispersion to near-infrared light (for 1310 nm and 1550 nm below 0.4 dB/km for) and having a high ability to sustain signal transmission rates (up to 40 Gbits/s in the applied system) <sup>20</sup>. The requirement for single-mode guidance for step index fiber designs is given by V, where V is defined as:

$$V = \frac{2\pi}{\lambda} a \sqrt{n_{core}^2 - n_{clad}^2} \quad (1)$$

By observing Eq. 1, V is a function of wavelength, meaning a single mode guide that can only be maintained over a limited wavelength range. For rays with smaller wavelengths beyond the cut-off wavelength, there will be

multiple modes within the fiber core. And the majority of SMF production is for use in the near-infrared wavelength range, with bandwidths around 1310 nm and 1550 nm.

### **2.1.2 Single-Mode Fiber**

A typical SMF core diameter is between 8 and 10  $\mu\text{m}$  with a 125  $\mu\text{m}$  cladding. SMF only supports a single mode in the fiber core. However, there are still a large number of cladding modes present in the cladding, because the fiber jacket boundary also forms the waveguide and will accommodate transmission of cladding modes that are inadvertently introduced into the fiber source end. The cladding modes of a typical SMF are often as short-lived as the core modes in MMF, whereby dispersion modes and leakage to the support coating will greatly weaken the transmission power and within a few centimeters along the longitudinal axis of the fiber can eliminate most of the cladding modes. The differences in the waveguide geometries result in the propagation constants of the core modes and cladding modes being different from each other, which ensures the integrity of the core modes in their propagation without significant interference from the co-propagating cladding modes.

However, Veng Sarkar *et al.* found that with gratings with a

periodicity in the hundreds of microns introduced into the fiber core, a practical method of interrupting the original propagation mode of the core mode, combining, and matching the phases with one or more cladding modes at the appropriate wavelengths. Can be seen in Fig. 2. Illustration of LPG interference in the original core mode propagation. Consequently, a power conversion will be made between the core modes and cladding modes, which would otherwise propagate independently and propagate under different patterns <sup>21-23</sup>. The core mode will lose most of its transmission power at the wavelengths where the mode coupling is formed, and therefore in the transmission spectrum a series of attenuation peaks is displayed. It was due to the strong weakening of the cladding mode.

The core and cladding modes include coupling which is useful in conveying information about ambient conditions and their variations in grating locations by light transmission. In addition, the phase matching conditions are highly sensitive to small variations of the grating period and the physical condition of the cladding layer, making fiber grating devices a suitable candidate for many fiber sensor applications.



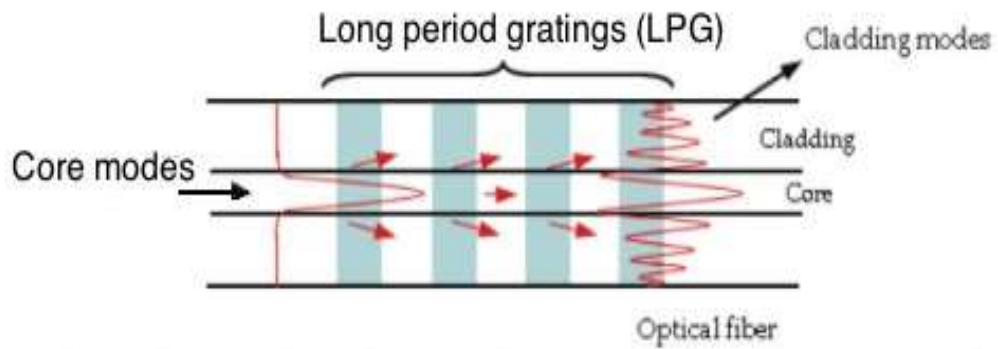


Figure 2. Illustration of disturbance in core mode propagation LPG.

The figure explained disturbed core mode is then phase-matched with one or more cladding modes and suffers a sharp loss in transmission power at the resonant wavelength. Image modified from Coelho *et al*<sup>24</sup>.

### 2.1.3 Double-Clad Fiber

The schematic cross-sectional views and refractive index profiles of the fabricated DCF are shown in Fig. 1. The radius of the core, inner cladding, and outer cladding in a step of the refractive index profile have values of 10  $\mu\text{m}$ , 125  $\mu\text{m}$  and 250  $\mu\text{m}$ , respectively. Based on this design, the beam above the cut-off wavelength of  $\sim 1100$  nm can be single-mode transmitted through the core and the beam launched into the inner cladding can be multimode guided due to the large-diameter DCF cladding area.

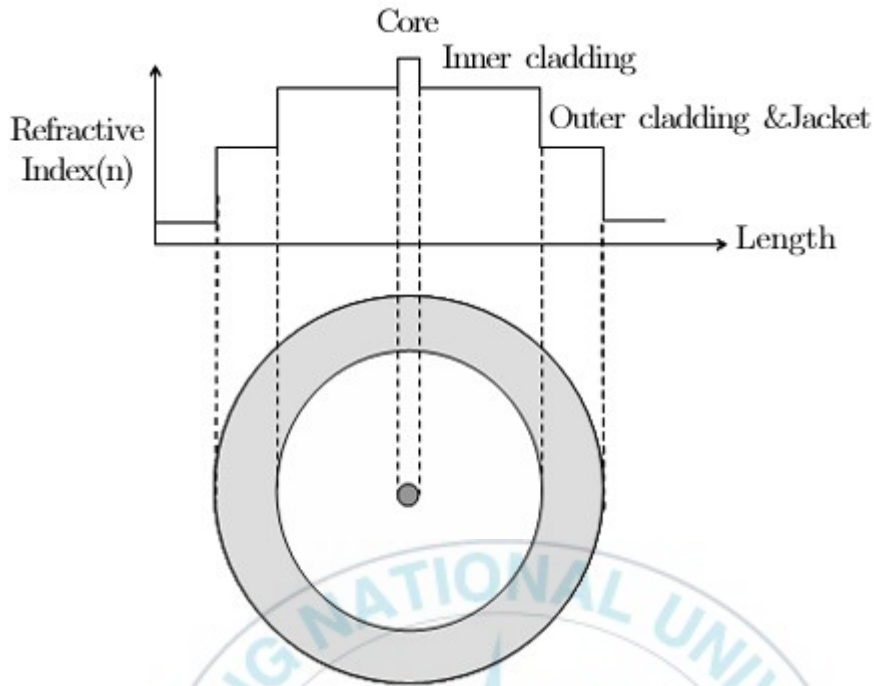


Figure 3. Refractive index profile (top) of a double-layered fiber (DCF) and schematic cross-sectional structure (bottom).

Since the conventional SMF has the same core and inner cladding sizes as the DCF, the loss of coupling between them is negligible.

## 2.2 Long Period Grating

Similar to Bragg grating, long period grating (LPG) is a structure that changes periodically along an optical fiber. The period is much larger, on the millimeter scale and for long-period gratings, it's generally easier to inscribe.

The inscribing can be directly on the cladding of the outer surface of the optical fiber. Meanwhile, Bragg grating acts as a mirror for light that propagates through the core mode, while the Long Period grating pairs light from the core mode to the cladding mode by propagating simultaneously. Because light cannot propagate efficiently in a cladding, meaning that it is scattered and attenuated quickly enough, Long Period Grating eliminates core wavelengths that are phase-matched to its period.

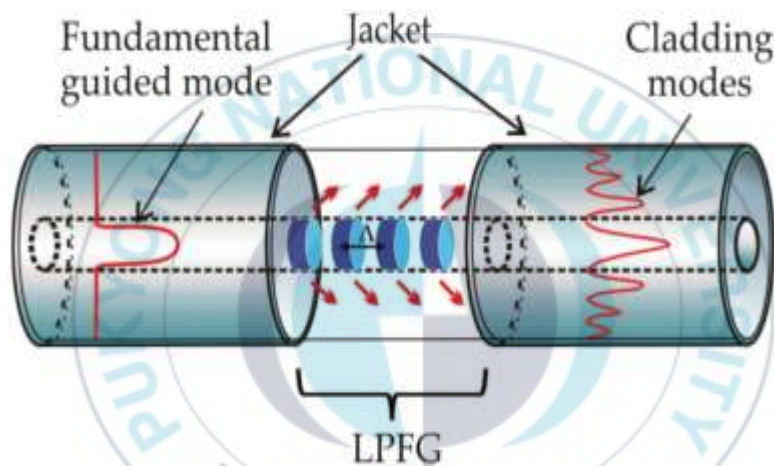


Figure 4. Schematic of the working principle of LPG.

The picture above explains light propagating through fiber. LPG changes the mode direction, and the core mode is coupled to the cladding mode. LPG acts as a wavelength filter because light cannot travel far through the cladding due to scattering, an image taken by Silva *et al.*<sup>25</sup>.

These two indicator dips are created due to the resonant coupling between the core mode and the cladding mode and have different cladding-mode orders. The phase-matching condition of a conventional LPFG can be described as:

$$\lambda_{res} = (n_{co,eff} - n_{cl,eff}) \Lambda, \quad (2)$$

where  $\lambda_{res}$  is the resonance wavelength;  $n_{co,eff}$  and  $n_{cl,eff}$  are the effective RIs of the fundamental core mode and cladding mode of the LPFG; and  $\Lambda$  is the grating pitch, respectively<sup>26</sup>. If LPG is stretched or bent and exposed to changes in temperature and humidity, the parameters of the coupling equation change resulting in a shift in wavelength. LPG is used in many applications, including band-pass filters, gain equalization, mode converters, attenuators, tunable filters, temperature, and strain sensors<sup>27</sup>. Most of the work has been done on silica fibers<sup>28-30</sup>. In LPG fabrication, grating periods range from 100  $\mu\text{m}$  - 1000  $\mu\text{m}$ <sup>31</sup>. LPG can be manufactured in various ways: LPG can be physically printed, UV inscribed<sup>32</sup>, made by electric arc discharge<sup>29</sup>, CO<sub>2</sub> laser inscribed<sup>30</sup>, made by acoustic waves and transient mechanical stress<sup>33,34</sup>.

### 2.3 LPFG Fabrication with CO<sub>2</sub> Laser

In its development, the use of CO<sub>2</sub> laser to write LPFG has emerged as an important alternative in LPFG fabrication. When compared to other fabrication methods, this technique provides many advantages, including lower insertion loss, higher flexibility, high thermal stability, and lower costs. In this section, the application of CO<sub>2</sub> laser irradiation in the manufacture of LPFG and also discussed the physical principles involved in the process. The earliest application of 10.6  $\mu\text{m}$  radiation by CO<sub>2</sub> laser beams in the manufacture of LPFG in conventional fibers was published in 1998<sup>35-37</sup>. And many different experimental methodologies have since been described. The most used method is the point-to-point technique using static asymmetric irradiation with a CO<sub>2</sub> laser that emits a specific mode (continuous wave, CW, or pulse) and a lens that focuses the beam on the fiber. Fig.5 shows a schematic of a typical LPFG fabrication system based on a point-to-point technique using a CO<sub>2</sub> laser. The optical fiber with its support stripped is placed in the motorized translation stage. During the writing process, the condition of the fibers is kept straight, when the laser beam is focused on the fiber, a small ballast is applied to the end of the fiber. This method has the advantage of requiring simpler adjustments, even though irradiation only

occurs on one side of the fiber. The write periodicity of the LPFG is accomplished by controlling the CO<sub>2</sub> laser beam emission and moving the fiber along its axial direction through a computer-controlled translation step. A broadband source and optical spectrum analyzer (OSA) are used to monitor spectrum evolution during laser irradiation. In addition, the motion of the translational stage can generate vibrations that can be transmitted to the fiber, affecting the repeatability and quality of the LPFG. This problem can be solved by using a system where the beam delivery system moves instead of fiber<sup>38</sup>. Several authors report hybrid methods, combining point-to-point and scanning<sup>39,40</sup>.

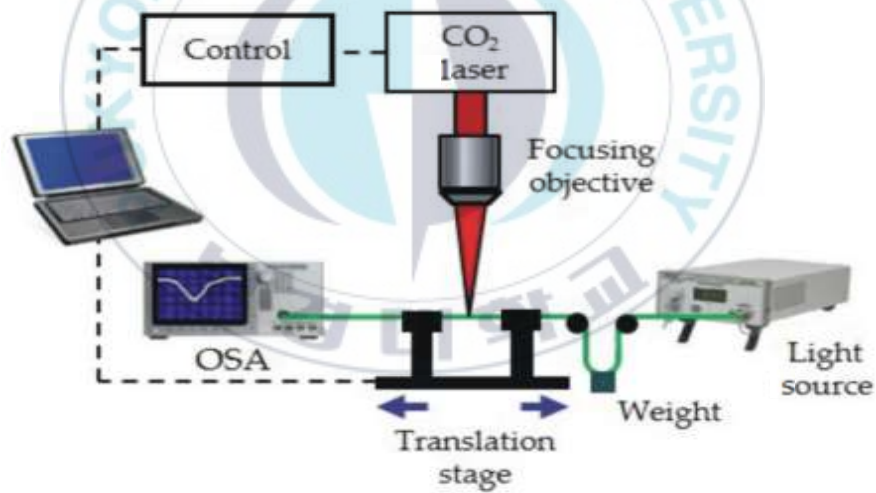
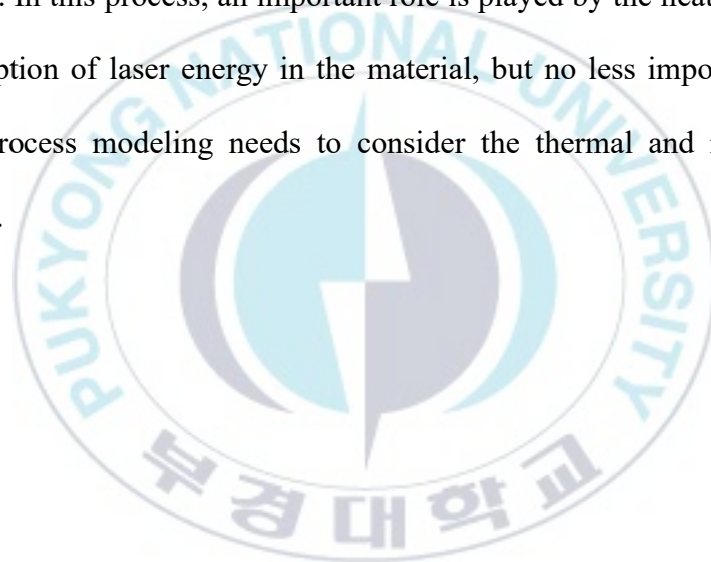


Figure 5. Schematic of a typical LPFG fabrication system based on a point-to-point technique using a CO<sub>2</sub> laser.



The symmetric cladding mode and the asymmetric cladding mode of the core mode coupling are due to the strong absorption power possessed by the silica glass around the wavelength of CO<sub>2</sub> laser radiation., the asymmetric RI modulation results from the emission intensity gradually attenuating along the direction of incidence <sup>41</sup>. This results in high polarization dependence loss which can be inevitable and high fiber grating birefringence <sup>42</sup>. To overcome the birefringence problem, different methods have been proposed. Zhu *et al.* <sup>43</sup> introduced an LPFG fabrication with uniform RI modulation with torsional strain to the fiber and then exposed both sides of the fiber to laser radiation using a high-frequency CO<sub>2</sub> laser system. Experimental results show that bent LPFGs (T-LPFGs) exhibit low insertion losses, clear spectra, and low polarization-dependent losses when compared to those created by single-sided CO<sub>2</sub> laser beam exposure <sup>44</sup>. Wang *et al.* <sup>45</sup> proposed a new method for writing asymmetric LPFGs using etching periodic grooves on one side of the fiber with a focused CO<sub>2</sub> laser beam. Because these grooves are completely confined within the cladding and do not affect the light transmission in the fiber core, the periodic grooves do not cause large insertion losses. The grooves improve grating fabrication efficiency and introduce unique optical properties with very high strain sensitivity. Using periodically deforming the

fiber geometry with a focused CO<sub>2</sub> laser beam and applying it to strain measurements. In 2006, Su *et al.*<sup>46</sup> introduced the possibility of generating long-period grating in multimode fiber. In addition to conventional single-mode fibers (SMFs), CO<sub>2</sub> lasers have been used to write LPFGs in other fiber types, such as boron-doped SMFs<sup>47,48</sup>, and photonic crystalline fibers (PCFs)<sup>49,50</sup>. Much of the understanding in the research focuses on the physical mechanisms involved in writing processes for various types of fibers with a CO<sub>2</sub> laser. In this process, an important role is played by the heat created by the absorption of laser energy in the material, but no less important is the writing process modeling needs to consider the thermal and mechanical processes.



### III. LPFG Fabrication

#### 3.1 Fabrication

This section will explain in detail the fabrication of long-period fiber gratings on double-clad fiber using a CO<sub>2</sub> laser and their responses to various physical parameters. Fig. 6. Schematic diagram of experimental setup Fabrication of long-period fiber gratings on double-clad fiber using CO<sub>2</sub> laser and Fig. 7 (a). shows a schematic diagram of the core and cladding structure of the Fabrication of long-period fiber gratings on double-clad fiber using a CO<sub>2</sub> laser. To make this sensor head, both ends of the DCF segment (Thorlabs, DCF 13) are connected to the SMF using a fusion splicer. The fiber arrangement becomes SMF-DCF-SMF. The sensor head was fabricated by irradiating a DCF segment with a 10.6  $\mu\text{m}$  CO<sub>2</sub> laser (Synrad, Inc.) using a line-by-line technique. Before irradiating by CO<sub>2</sub> laser, one end of the DCF-LPFG was fixed on the fiber holder, and the other end was suspended with a 10 g weight to make a slight longitudinal tension to the fiber. The pulse output from a laser whose pulse width is modulated at 20 kHz with a duty ratio of 5.5% has a maximum peak power of  $\sim 30$  W and an average power of  $\sim 2.78$  W. A beam expander is used to increase the output beam diameter, and the expanded beam is focused by a lens  $f-\theta$  ending with a point diameter of

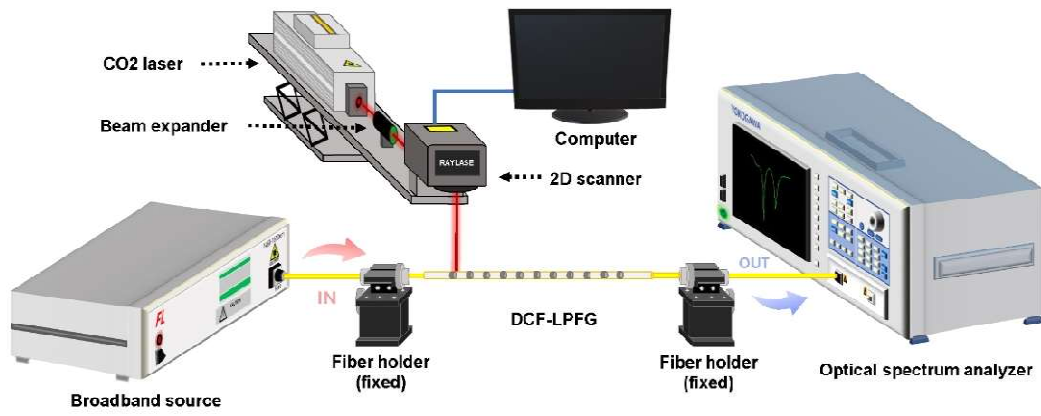


Figure 6. Schematic diagram for fabrication of long-period fiber gratings on double-clad fiber using a CO<sub>2</sub> laser.

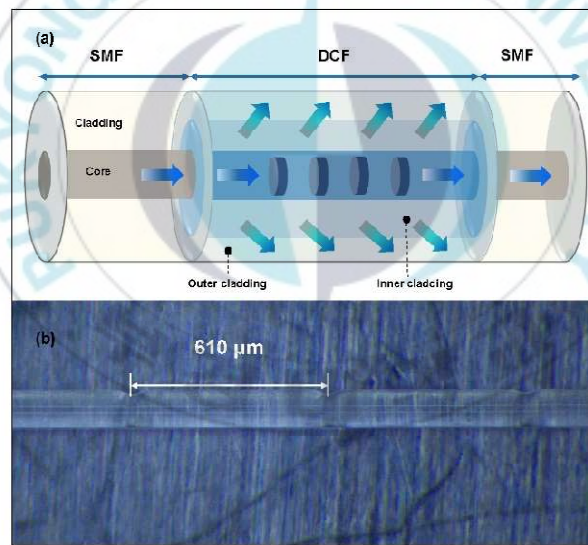


Figure 7. (a) Schematic diagram of core and cladding structure of DCF-LPFG and (b) optical microscope image of fabricated DCF-LPFG.

~68  $\mu\text{m}$ . Then, we performed a focused beam scan of the DCF segment using a 2D optical scanner. The fabrication parameters for the DCF-LPFG, such as beam scanning power, scanning speed, grating pitch ( $\Lambda$ ), and grating periods, which can be set electronically and modified with a dedicated computer, are 3.82 W, ~30 mm/s, 610  $\mu\text{m}$ , and 35 grating periods. Fig. 7(b) shows the optical microscopy image of the center region of the fabricated DCF-LPFG with a 21 mm grating length. As seen in Fig. 2(b), we can see the periodic etched dots on the fiber surface, which are formed by CO<sub>2</sub> laser scanning based on the point-to-point technique.

### 3.2 Transmission Characteristics

Fig. 8, shows the transmission spectrum of the fabricated long-period fiber gratings on double-clad fiber, measured at room temperature without any applied physical parameters. The transmission spectrum of the fabricated sensor head was monitored by using an optical spectrum analyzer (OSA, Yokogawa AQ6370C) and a broadband light source (BBS, Fiberlabs FL7001). In the transmission spectrum, the sensor head has an insertion loss of -0.97 dB and an extinction ratio of -34.65 dB. This sensor head also generates two attenuation dips, whose resonance wavelengths were ~1508.62

nm and  $\sim 1551.88$  nm, which were selected as sensor indicator dips denoted by Dip A and Dip B, respectively. These two indicator dips are created due to the resonant coupling between the cladding mode and the core mode and have different cladding-mode orders. The typical transmission spectrum showed a low insertion loss ( $<1$ dB) and a high extinction ratio ( $>25$ dB), which would be perfectly adequate for most fields of communication and sensing.

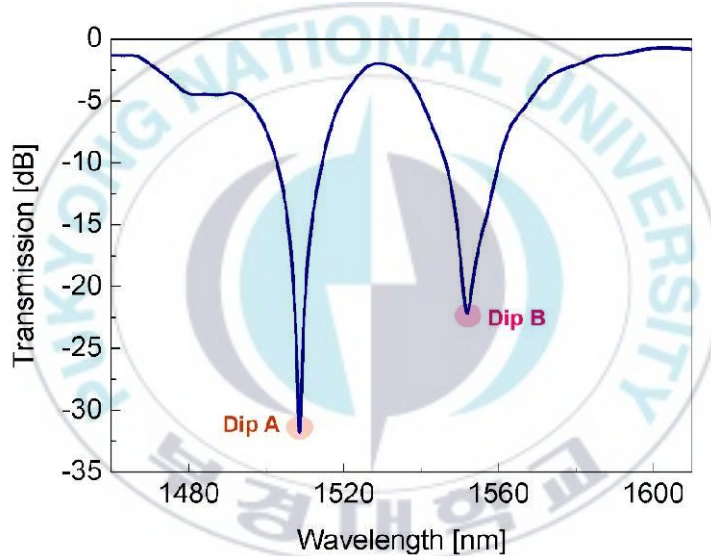


Figure 8. Transmission spectrum of fabricated DCF-LPFG measured at room temperature without any applied strain or torsion.



## **IV. Experimental Preparation and Measurement Results**

### **4.1 Experiment Setup**

Fig. 9 to Fig. 12 shows a schematic diagram of the experimental setup designed to investigate the physical parameters responses of the fabricated DCF-LPFG. Physical parameters to be measured include bending, strain, torsion, and temperature. To monitor the physical parameters responses of the DCF-LPFG, we employed a broadband light source (Fiberlabs FL7701) with an output wavelength range from S to L bands and an optical spectrum analyzer (Yokogawa AQ6370C) with a resolution bandwidth of 0.02 nm.

#### **4.1.1 Bending Measurement**

First, the bending response of the fabricated DCF-LPFG was investigated by using an experimental setup as shown in Fig. 9, the figure shows schematic diagrams of the experimental setups designed to investigate the bending responses of the fabricated DCF-LPFG. The BBS and OSA were employed to monitor the bending and temperature responses of the sensor. First, to investigate the bending response Dip A and Dip B of the fabricated DCF-LPFG, one end of the sensor head was attached to a fixed fiber holder, and its other end was fixed to a rotatable fiber holder attached to a translation

stage. The bending could be applied to the sensor segment by moving the translation stage in the CW direction of the rotatable fiber holder, as shown in Fig.8 the applied bending could be varied by minutely adjusting the longitudinal displacement ( $\Delta L$ ) of the translation stage. The applied bending is quantitatively represented as the curvature  $C = 1/R$ , where  $R$  is the radius of curvature of the fiber segment that contains the DCF-LPFG, which is also expressed as  $C = (24\Delta L/L_0^3)^{1/2}$ , where  $L_0$  (, set at  $\sim 100$  mm here,) is the initial distance between the fixed fiber holder and the translation stage. This bending measurement is measured in the curvature range of  $0.0$  to  $1.22 \text{ m}^{-1}$  at room temperature ( $\Delta T = 0$ )

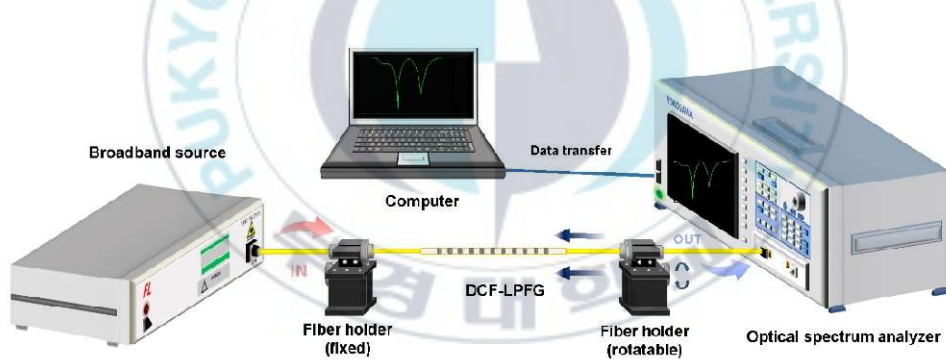


Figure 9. Schematic diagram of experimental setup designed to investigate bending responses of fabricated sensor head (DCF-LPFG).

#### 4.1.2 Strain Measurement

Next, we also scrutinized the strain-induced spectral changes of Dip A and Dip B in an applied strain range from 0 to 2000  $\mu\epsilon$ , at room temperature ( $\Delta T = 0$ ) using the same experimental setup as used in the investigation of the bending responses. During the scrutinization, the longitudinal strain was applied to the sensor segment by gently moving the fiber holder on the translation stage shown in Fig 10.

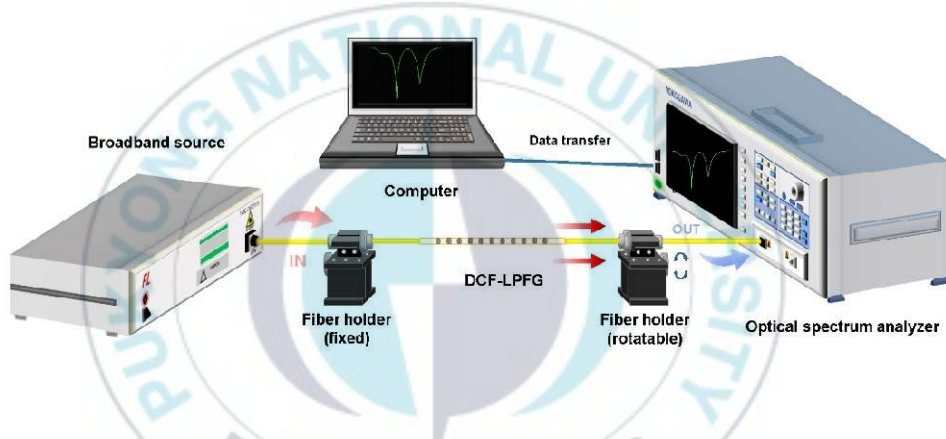


Figure 10. Schematic diagram of experimental setup designed to investigate strain responses of fabricated sensor head (DCF-LPFG).

#### 4.1.3 Torsion Measurement

Then, the torsion response of the fabricated sensor was investigated by attaching one end of the sensor head to a fixed fiber holder and the other one

to a rotatable fiber holder. Torsion was applied to the DCF-LPFG by gradually rotating the fiber rotator located in the fiber holder in the CW or CCW direction, as shown in Fig. 11. A twist rate  $\tau$  is given by  $\theta/L$ , where  $\theta$  is the rotation angle of the fiber rotator, and  $L$  is the distance between the two fiber holders (i.e., fixed and rotatable fiber holders). Here, the distance  $L$  was  $\sim 0.18$  m. This torsion measurement is measured in the twist range of  $-180^\circ$  to  $180^\circ$  with a step of  $45^\circ$  at room temperature ( $\Delta T = 0$ ).

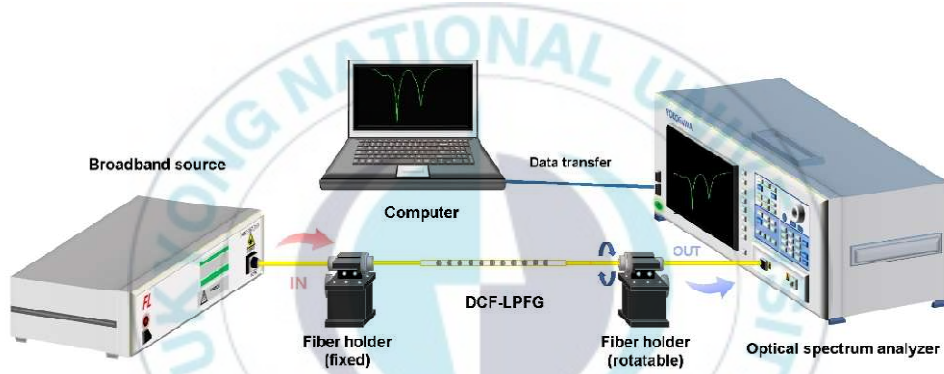


Figure 11. Schematic diagram of experimental setup designed to investigate torsion responses of fabricated sensor head (DCF-LPFG).

#### 4.1.4 Temperature Measurement

Finally, to observe the temperature responses of the sensor indicators Dip A and Dip B of the fabricated DCF-LPFG, the sensor head was placed

on a hot plate, and the temperature-induced spectral variations of the two indicator dips were investigated in a temperature range from 25 to 100 °C (step: 5 °C) without applied torsion ( $\Delta\tau = 0$ ). During the characterization of the temperature response, a small amount of longitudinal tension was applied to the sensor segment to avoid the thermally induced micro bending of the sensing fiber. To provide a stable temperature environment, a thermal chamber made of enclosed aluminum foil was utilized to explore the temperature response of the DCF-LPFG located within the chamber. As seen in Fig. 12, an electronic thermometer (Fluke 51 II) was used to monitor the temperature inside the thermal chamber.

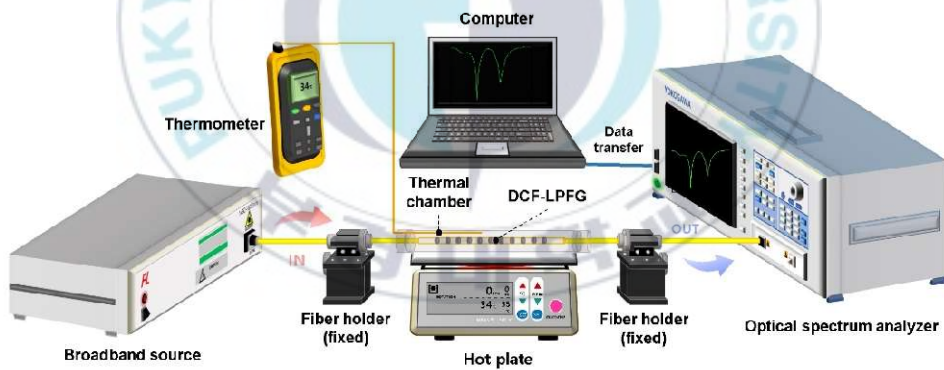


Figure 12. Schematic diagram of experimental setup designed to investigate temperature responses of fabricated sensor head (DCF-LPFG).

## 4.2 Measurement Results

### 4.2.1 Bending Measurement Results

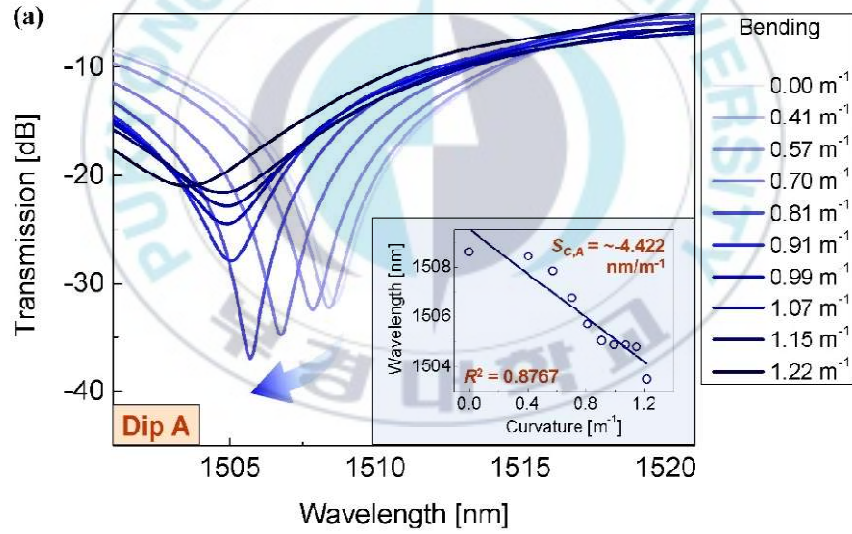
Figs. 13 (a) and (b) show bend-induced spectral variations of Dip A and Dip B of the DCF-LPFG, Dip A and Dip B moved towards a shorter wavelength region (in the direction of the blue arrow) showing a blue shift. When the applied bending ( $\Delta C$ ) was changed from 0.0 to 1.22 m<sup>-1</sup> corresponding to a  $\Delta L$  range from 0.0 to 1.22 m<sup>-1</sup>,  $\lambda_A$  of Dip A decreased from ~1508.62 to ~1503.52. For the same  $\Delta C$  range from 0.0 to 1.22 m<sup>-1</sup> as in Dip A,  $\lambda_B$  of Dip B decreased from ~1551.88 to ~1530 nm, exhibiting a blue shift. A bend-induced change in  $\lambda_A$  or  $\lambda_B$  is attributed to bend-induced changes in the effective refractive index difference  $\Delta n_{eff}$  and the grating pitch. The bending sensitivity of the DCF-LPFG can be drawn out from (2) and is given by <sup>51</sup>

$$\frac{\partial \lambda_{dip}}{\partial C} = \lambda_{dip} \left( \frac{1}{\Delta n_{eff}} \frac{\partial \Delta n_{eff}}{\partial C} + \frac{1}{\Lambda} \frac{\partial \Lambda}{\partial C} \right) \quad (3)$$

where  $C$  and  $\Delta n_{eff} (= n_{co,eff} - n_{cl,eff})$  represent the curvature and the difference between the effective refractive indices of the core and cladding, respectively. The bending sensitivities of Dip A and Dip B, that is,  $S_{\tau A}$  and  $S_{\tau B}$  were measured as approximately -4.422 nm/m<sup>-1</sup> and -21.88 nm/m<sup>-1</sup>, respectively.

It is noted that the magnitude of  $S_{CB}$  was 5 times greater than that of  $S_{CA}$ . The magnitude difference between  $S_{CA}$  and  $S_{CB}$  seems to originate from the cladding-mode order difference between Dip A and Dip B.

The inset of Figs. 13(a) and 13(b) display the bending-induced wavelength shifts of Dip A and Dip B for the applied strain ranging from 0.0 to  $1.22 \text{ m}^{-1}$ , respectively. Blue circular symbols and solid lines in both insets represent the measured values of indicator dip wavelengths and the linear fits of the measured data of  $\lambda_A$  and  $\lambda_B$ , respectively





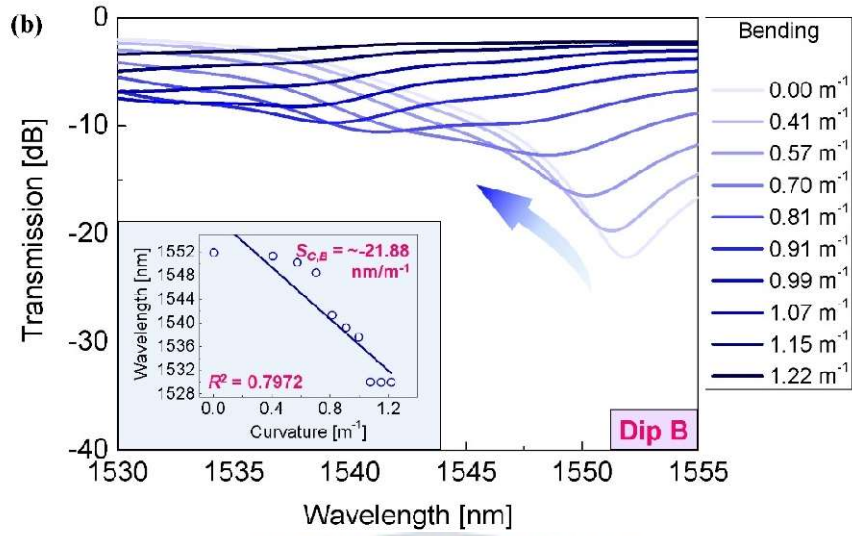


Figure 13. Spectral variations of sensor indicators (a) Dip A and (b) Dip B, induced by applied bending of 0.0 to 1.22 m<sup>-1</sup>. The inset of (a) and (b) show the bend-induced wavelength shifts of Dip A and Dip B, respectively.

#### 4.2.2 Strain Measurement Results

Figs 14(a) and 14(b) show the strain-induced spectral variations of the two sensor indicators (i.e., Dip A and Dip B), measured for an applied strain range of 0 to 2000  $\mu\epsilon$  (step:  $\sim 222.2 \mu\epsilon$ ) at room temperature ( $\Delta T = 0$ ) without any applied torsion ( $\Delta \tau = 0$ ), respectively. As seen in Figs. 14(a) and 14(b), Dip A and Dip B exhibited very slight blue shifts and blue shifts of  $\sim 0.32$  and  $\sim 1.12$  nm with increasing strain along the sensing fiber, respectively.

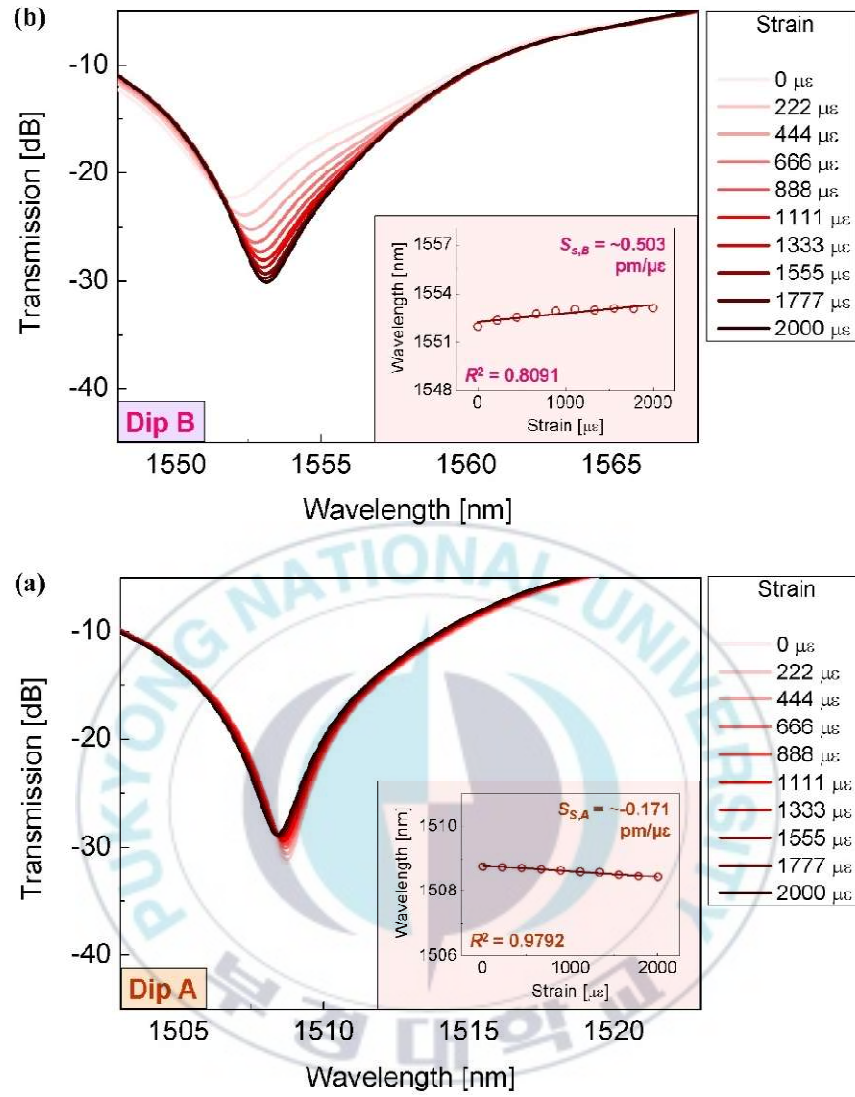


Figure 14. Spectral variations of sensor indicators (a) Dip A and (b) Dip B, induced by applied strain of 0 to 2000  $\mu\epsilon$ . The insets of (a) and (b) show the strain-induced wavelength shifts of Dip A and Dip B, respectively.

The inset of Figs. 6(a) and 6(b) display the strain-induced wavelength shifts of Dip A and Dip B for the applied strain ranging from 0 to 2000  $\mu\epsilon$ , respectively. Red circular symbols and solid lines in both insets represent the measured values of indicator dip wavelengths and the linear fits of the measured data of  $\lambda_A$  and  $\lambda_B$ , respectively. Based on the results, the strain sensitivities of Dip A and Dip B, designated as  $S_{SA}$  and  $S_{SB}$ , were evaluated as approximately  $-0.171$  and  $5.029$  pm/ $\mu\epsilon$ , respectively. However, the adjusted  $R^2$  values of Dip A and Dip B were  $\sim 0.9792$  and  $\sim 0.8091$ , respectively, which implies that their strain responses are good linear. The bending sensitivity of the sensor head can be drawn out from (2) and is given by <sup>52</sup>.

$$\frac{\partial \lambda_{dip}}{\partial s} = \lambda_{dip} \left( \frac{1}{\Delta n_{eff}} \frac{\partial \Delta n_{eff}}{\partial s} + \frac{1}{\Lambda} \frac{\partial \Lambda}{\partial s} \right) \quad (4)$$

where  $C$  and  $\Delta n_{eff}$  ( $= n_{co,eff} - n_{cl,eff}$ ) represent the curvature and the difference between the effective refractive indices of the core and cladding, respectively.

#### 4.2.3 Torsion Measurement Results

Figs 15(a) and 15(b) show spectral variations of Dip A and Dip B caused by torsion, measured at room temperature ( $25^\circ\text{C}$ ,  $\Delta T = 0$ ), respectively. The torsion-induced spectral changes of Dip A and Dip B were

recorded while varying the twist angle from  $-180^\circ$  to  $180^\circ$  with a step of  $45^\circ$ . Here, plus and minus twist angles imply that torsion is applied to the sensor in the CW and CCW directions, respectively. The two indicator dips moved towards a longer wavelength region showing redshifts. Specifically,  $\lambda_A$  increased from 1506.16 to 1510.22 nm ( $\Delta\lambda_A = -4.06$  nm), and  $\lambda_B$  increased from 1550.54 to 1552.46 nm ( $\Delta\lambda_B = -1.92$  nm). These torsion-induced changes in  $\lambda_A$  and  $\lambda_B$  are caused by torsion-induced changes in  $\Delta n_{eff}$  ( $= n_{co, eff} - n_{cl, eff}$ ) and  $\Lambda$ . From (2), the torsion sensitivity of the DCF-LPFG is obtained as <sup>53</sup>

$$\frac{\partial \lambda_{dip}}{\partial \tau} = \lambda_{dip} \left( \frac{1}{\Delta n_{eff}} \frac{\partial \Delta n_{eff}}{\partial \tau} + \frac{1}{\Lambda} \frac{\partial \Lambda}{\partial \tau} \right), \quad (5)$$

where  $\lambda_{dip}$  is the dip wavelength of the sensor indicator, and  $\partial \lambda_{dip} / \partial \tau$  is the rate of change of the indicator dip wavelength with respect to the applied torsion, i.e., the torsion sensitivity of the indicator dip. The second term on the right-hand side of (5) is close to zero because the grating period rarely changes with the applied torsion irrespective of the twist direction. Accordingly, the torsion-induced variation in the effective RI difference  $\Delta n_{eff}$  dominantly affects the torsion-induced wavelength shift in the indicator dip and thus the torsion sensitivity.

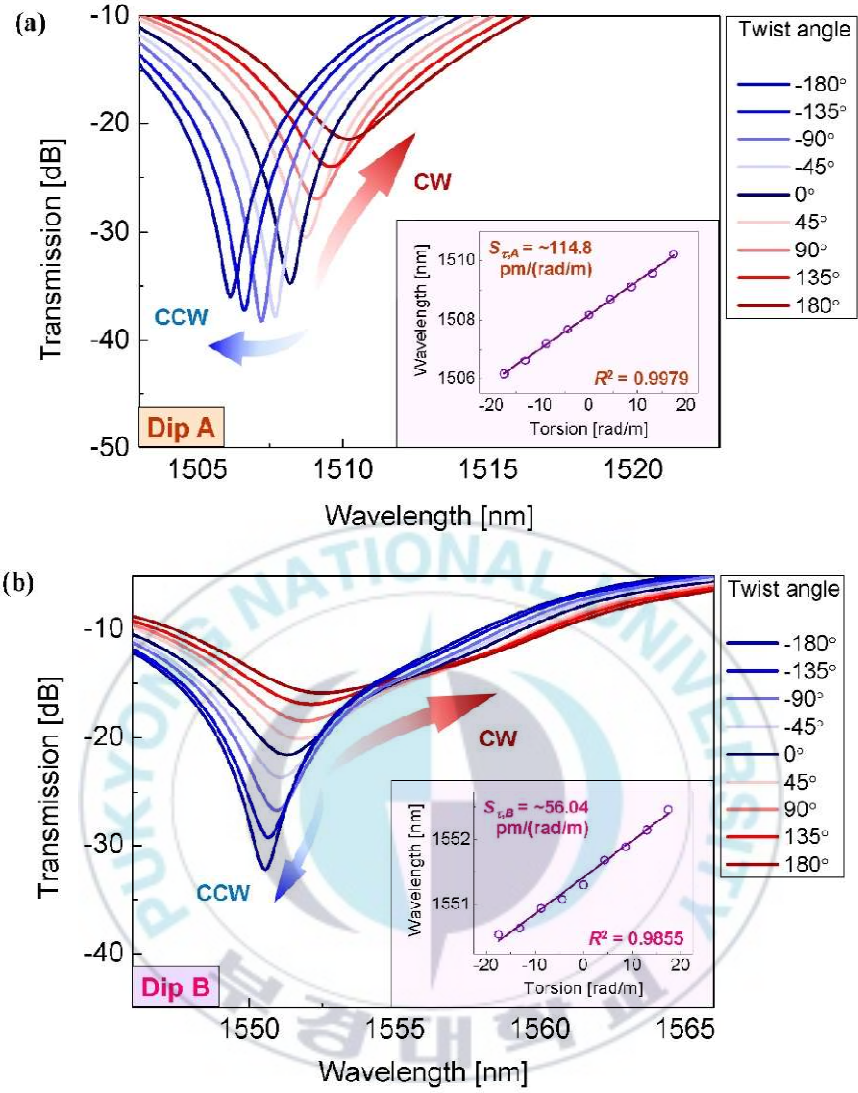


Figure 15. Spectral variations of sensor indicators (a) Dip A and (b) Dip B, induced by applied twist of  $-180^\circ$  to  $180^\circ$ . The insets of (a) and (b) show the torsion-induced wavelength shifts of Dip A and Dip B, respectively.

The torsion sensitivities of Dip A and Dip B, that is,  $S_{\tau A}$  and  $S_{\tau B}$ , were measured as approximately 114.80 and 56.04 pm/(rad/m), respectively. It is noted that the magnitude of  $S_{\tau A}$  was 2.0 times greater than that of  $S_{\tau B}$ . The magnitude difference between  $S_{\tau A}$  and  $S_{\tau B}$  seems to originate from the cladding-mode order difference between Dip A and Dip B.

The insets of Figs. 4(a) and 4(b) show the torsion-induced wavelength shifts of Dip A and Dip B, represent the measured values of indicator dip wavelengths and the linear fits of the measured data of  $\lambda_A$  and  $\lambda_B$ , respectively measured for the applied torsion variation ranging from  $-9.69$  to  $9.69$  rad/m, respectively.

#### 4.2.4 Temperature Measurement Results

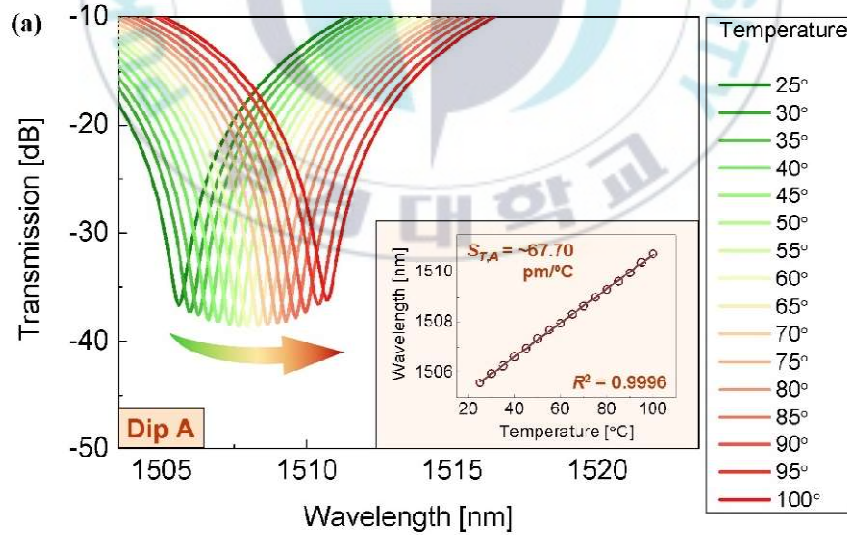
Figs. 16(a) and 16(b) show temperature-induced spectral variations of two sensor indicators Dip A and Dip B, measured in a temperature range from 25 to 100 °C without any applied torsion ( $\Delta\tau = 0$ ). We found from the figure that Dip A and Dip B moved towards a longer wavelength region showing redshifts from 1505.58 to 1510.72 nm and from 1550.8 to 1555.98 nm, respectively. Likewise in the case of the other parameter wavelength shifts of Dip A and Dip B, these temperature-induced redshifts in  $\lambda_A$  and  $\lambda_B$  are also



caused by thermally induced changes in  $\Delta n_{eff}$  and  $\Lambda$  <sup>51</sup>. Similarly, the temperature sensitivity of the DCF-LPFG is given by

$$\frac{\partial \lambda_{dip}}{\partial T} = \lambda_{dip} \left( \frac{1}{\Delta n_{eff}} \frac{\partial \Delta n_{eff}}{\partial T} + \frac{1}{\Lambda} \frac{\partial \Lambda}{\partial T} \right), \quad (6)$$

where  $\partial \lambda_{dip} / \partial T$  is the temperature sensitivity of the indicator dip. The first term on the right-hand side of (6), which depends on the product of the inverse of  $\Delta n_{eff}$  and  $\partial \Delta n_{eff} / \partial T$ , refers to the thermo-optic effect in  $\Delta n_{eff}$ . The second term is associated with the silica thermal expansion and can usually be neglected because it is some orders of magnitude smaller than the first one <sup>52</sup>. The temperature sensitivities of Dip A and Dip B, that is,  $S_{TA}$  and  $S_{TB}$  were measured as  $\sim 67.70$  and  $\sim 67.44$  pm/°C, respectively.





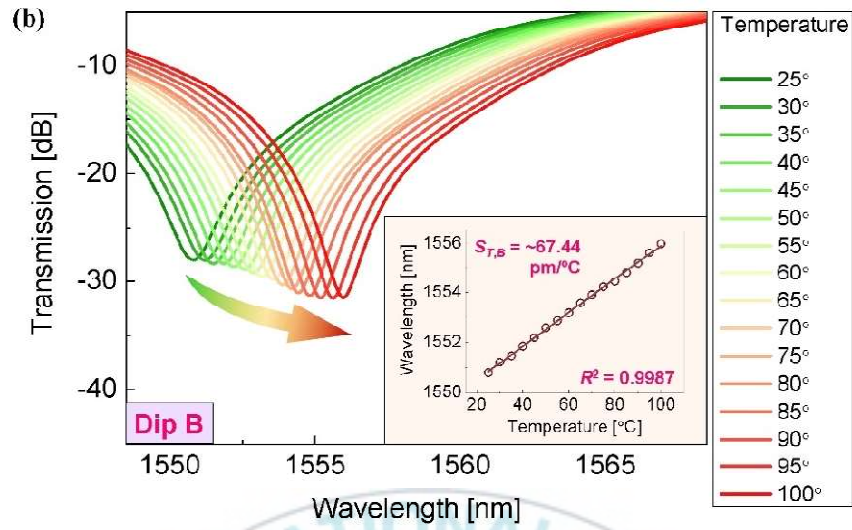


Figure 16. Spectral variations of sensor indicators (a) Dip A and (b) Dip B, induced by applied temperature of 25 to 100 °C. The insets of (a) and (b) show the thermal-induced

Similarly, the insets of Figs. 16(a) and 16(b) display the temperature-induced wavelength shifts of Dip A and Dip B, measured for the applied temperature variation ranging from 25 to 100 °C, respectively

## V. Conclusion

In summary, we experimentally demonstrated an optical fiber sensor capable of measuring various physical parameters by incorporating a DCF-LPFG. The DCF-LPFG as a sensor head was fabricated by scanning CO<sub>2</sub> laser pulses on DCF with a uniform period. In the transmission spectrum of the fabricated sensor head, two attenuation dips whose resonance wavelengths were  $\lambda_A = \sim 1508.62$  nm and  $\lambda_B = \sim 1551.88$  nm were selected as sensor indicators (Dip A and Dip B, respectively) for the measurement of bending, strain, torsion, and temperature variations. For both sensor indicators, their physical parameter responses were investigated in a bending curvature range of 0.0 to 1.22 m<sup>-1</sup>, twist range of 0 to 2000  $\mu\epsilon$ , a twist angle range of  $-180^\circ$  to  $180^\circ$  and a temperature range of 25 to 100 °C, respectively. The bending sensitivities of Dip A and Dip B were measured to be approximately -4.422 and -21.88 nm/m<sup>-1</sup>, the strain sensitivities of Dip A and Dip B were measured to be approximately -0.171 and 5.029 pm/ $\mu\epsilon$ , the torsion sensitivities of Dip A and Dip B were measured to be approximately 114.80 and 56.04 pm/(rad/m), and the temperature sensitivities of Dip A and Dip B were measured to be  $\sim 67.70$  and  $\sim 67.44$  pm/°C, respectively. The DCF-LPFG response from the measurement of 4 physical parameters showed good performance. However,

the bending measurement showed poor data sensitivity. In measuring these physical parameters, the factor that determines sensor performance is the influence of the effective RI of the cladding and the effective RI of the core. This is it can be exemplified when a physical parameter such as torsion is applied to the LPFG, because the core hardly depends on torsion, the effective RI of the cladding is significantly changed compared with the effective RI of the core, resulting in a change in the resonance condition and a resonance wavelength shift, and the same applies to other physical parameters. From the fabrication and experimental we show, its ability to discriminate 4 physical parameters, shows a sensitive and insensitive response. So, it can potentially simultaneously measure 2 or more physical parameters for future work. The proposed DCF-LPFG is expected to be beneficial as a compactly embedded and electrically passive cost-effective sensor head for structural health monitoring in various industrial trial applications.

## References

1. L. Eldada, "Optical communication components," Rev. Sci. Instrum, vol. 75, pp. 575593, 2004, <https://doi.org/10.1063/1.1647701>
2. Y. -G. Han, S. Kim, and S. Lee, "Flexibly tunable multichannel filter and bandpass filter based on long-period fiber gratings," Opt. Express, vol. 12, no. 9, pp. 1902-1907, 2004, <https://doi.org/10.1364/OPEX.12.001902>
3. H. An, B. Ashton, and S. Fleming, "Long-period-grating-assisted optical add-drop filter based on mismatched twin-core photosensitive-cladding fiber," Optics Letters, vol. 29, no. 4, pp. 343-345, 2004, <https://doi.org/10.1364/ol.29.000343>
4. B. J. Eggleton, R. E. Slusher, J. B. Judkins, J. B. Stark, and A. M. Vengsarkar, "Alloptical switching in long-period fiber gratings," Optics Letters, vol. 22, no. 12, pp. 883-885, 1997 <https://doi.org/10.1364/ol.22.000883>
5. R. Slavík, "Extremely deep long-period fiber grating made with CO<sub>2</sub> laser,". IEEE Photonics Technology Letters, vol. 18, no. 16, pp.1705–1707, 2006, <https://doi.org/10.1109/LPT.2006.879924>

6. J.M. Lopez-Higuera, L.R. Cobo, A.Q. Incera, and A. Cobo, "Fiber optic sensors in structural health monitoring," *Journal of Lightwave Technology*, vol. 29, no. 4, pp. 587–608, 2011, <https://doi.org/10.1016/j.jprotcy.2016.08.065>
7. R.R. Kim, and J.P. Edward, "Fiber optic sensors for environmental monitoring," *Chemosphere*, vol. 33, no. 6, pp.1151–1174, 1996. <https://doi.org/10.15626/Eco-Tech.1999.062>
8. K. O. Hill and G. Meltz, "Fiber Bragg grating technology: Fundamentals and overview," *Journal of Lightwave Technology*, vol. 15, no. 8, pp. 1263–1276, 1997. <https://doi.org/10.1109/50.618320>
9. T. Erdogan, "Fiber grating spectra," *Journal of Lightwave Technology*, vol. 15, no. 8, pp. 1277–1294, 1997. <https://doi.org/10.1109/50.618322>
10. A. M. Vengsarkar, P. J. Lemaire, J. B. Judkins, V. Bhatia, T. Erdogan, and J. E. Sipe, "Long-period fiber gratings as band-rejection filters," *J. Lightwave Technol.*, vol. 14, pp. 58–65, 1996, <https://doi.org/10.1364/OFC.1995.PD4>
11. Q. Li, C.-H. Lin, A. A. Au, and H. P. Lee, "Compact all-fibre on-line

- power monitor via core-to-cladding mode coupling,” *Electronics Letters*, vol. 38, pp. 1013-1015, Aug. 29, 2002, <https://doi.org/10.1049/el:20020674>
12. S. Liu, Y. Zhang, C. Fu, Z. Bai, Z. Li, C. Liao, Y. Wang, J. He, Y. Liu, and Y. Wang, “Temperature insensitivity polarization-controlled orbital angular momentum mode converter based on an LPFG induced in four-mode fiber,” *Sensors*, vol. 18, no. 6, p. 1766, 2018. <https://doi.org/10.3390/s18061766>
13. M. Deng, J. Xu, Z. Zhang, Z. Bai, S. Liu, Y. Wang, Y. Zhang, C. Liao, W. Jin, G. Peng, and Y. Wang, “Long-period fiber grating based on periodically screw-type distortions for torsion sensing,” *Optics Express*, vol. 25, no. 13, pp. 14308–14316, 2017. <https://doi.org/10.1364/OE.25.014308>
14. Y.-S. Zhang, W.-G. Zhang, L. Chen, Y.-X. Zhang, S. Wang, L. Yu, Y.-P. Li, P.-C. Geng, T.-Y. Yan, X.-Y. Li, and L.-X. Kong, “Concave-lens-like long-period fiber grating bidirectional high-sensitivity bending sensor,” *Optics Letters*, vol. 42, no. 19, pp. 3892–3895, 2017. <https://doi.org/10.1364/OL.42.003892>

15. J. Tang, Z. Zhang, G. Yin, S. Liu, Z. Bai, Z. Li, M. Deng, Y. Wang, C. Liao, J. He, W. Jin, G.-D. Peng, and Y. Wang, "Long-period fiber grating inscribed in hollow-core photonic bandgap fiber for gas pressure sensing," *IEEE Photonics Journal*, vol. 9, no. 5, pp. 1–7, 2017. <https://doi.org/10.1109/JPHOT.2017.2738666>
16. H. C. A. S. G. Vasconcelos, J. M. M. M. d. Almeida, C. M. T. Saraiva, P. A. d. S. Jorge, and L. C. C. Coelho, "Mach-Zehnder interferometers based on long-period fiber grating coated with titanium dioxide for refractive index sensing," *Journal of Lightwave Technology*, vol. 37, no. 18, pp. 4584–4589, 2019. <https://doi.org/10.1109/JLT.2019.2912829>
17. D.D. Davis, T.K. Gaylord, E.N. Glytsis, S.G. Kosinski, S.C. Mettler, and A.M. Vengsarkar, "Long-period fibre grating fabrication with focused CO<sub>2</sub> laser pulses," *Electronics Letters*, vol. 34, pp. 302-303, 1998. <https://doi.org/10.1049/el:19980239>
18. Y.J. Rao, Y.P. Wang, Z.L. Ran, and T. Zhu, "Novel Fiber-Optic Sensors Based on Long-Period Fiber Gratings Written by High-Frequency CO<sub>2</sub> Laser Pulses," *Journal of Lightwave Technology*. vol.



- 21, pp. 1320-1327, 2003. <https://doi.org/10.1109/JLT.2003.810561>
19. D. Nikogosyan, "Multi-photon high-excitation-energy approach to fiber grating inscription," *Measurement, Science and Technology*, vol. 28, pp. R1–R29, 2007. <http://dx.doi.org/10.1088/0957-0233/18/1/R01>
20. S. Yao, "Polarization in Fiber Systems: Squeezing Out More Bandwidth", *The Photonics Handbook*, p. 1. Laurin Publishing, 2003.
21. A. M. Vengsarkar, P. J. Lemaire, J. B. Judkins, V. Bhatia, T. Erdogan, and J. E. Sipe, "Long-period fiber gratings as band-rejection filters," *Journal of Lightwave Technology*, vol.14, p. 58, 1996. <https://doi.org/10.1364/OFC.1995.PD4>
22. K. O. Hill, B. Malo, K. Vineberg, F. Bilodeau, D. Johnson, and I. Skinner, "Efficient mode-conversion in telecommunication fiber using externally written gratings," *Electronics Letters*, vol. 26, pp. 1270–1272, 1990. <https://doi.org/10.1049/el:19900818>
23. F. Bilodeau, K. O. Hill, B. Malo, and D. Johnson, "Efficient narrowband  $lp_{01}$  to  $lp_{02}$  mode conversion fabricated in photosensitive fiber: Spectral response," *Electronics Letters*, vol. 27, pp. 682–684, 1991. <https://doi.org/10.1049/el:19910426>

24. J. M. P. Coelho, M. Nespereira, C. Silva, D. Pereira, and J. Rebordo, Current Developments in Optical Fiber Technology, ch. Advances in Optical Fiber Laser Micromachining for Sensors Development. InTech, 2013. <https://doi.org/10.5772/52745>
25. C. Silva, J. Coelho, P. Caldas, and P. Jorge, “Fibre Sensing System Based on Long-Period Gratings for Monitoring Aqueous Environments,” Fiber Optic Sensors, pp. 317–342, 2012. <https://doi.org/10.5772/27372>
26. V. Budinski and D. Donlagic, “Fiber-optic sensors for measurements of torsion, twist, and rotation: A review,” Sensors, vol. 17, no. 3, p. 443, 2017. <https://doi.org/10.3390/s17030443>
27. M. A. Van Eijkelenborg, W. Padden, and J. A. Besley, “Mechanically induced long-period gratings in microstructured polymer fiber,” Optic Communications, vol. 236, pp. 75–78, 2004. <http://dx.doi.org/10.1016/j.optcom.2004.03.004>
28. B. Eggleton, C. Kerbage, P. Westbrook, R. Windeler, and A. Hale, “Microstructured optical fiber devices,” Optics Express, vol. 9, pp. 698-713, 2001. <https://doi.org/10.1364/OE.9.000698>

29. G. Humbert, A. Malki, S. Février, P. Roy, and D. Pagnoux, "Electric arc-induced long-period gratings in Ge-free air-silica microstructure fibers," *Electronics Letters*, vol. 39, p. 349 2003. <https://doi.org/10.1049/el:20030271>
30. G. Kakarantzas, T. a Birks, and P. S. J. Russell, "Structural long-period gratings in photonic crystal fibers," *Optics Letters*, vol. 27, pp. 1013–101, 2002. <https://doi.org/10.1364/OL.27.001013>
31. J. M. P. Coelho, C. Silva, M. Nespereira, M. Abreu, and J. Rebordão, "Writing of Long Period Fiber Gratings Using CO<sub>2</sub> Laser Radiation," *Advances in Optical Fiber Technology, Fundamental Optical Phenomena Application*, 2015. <https://doi.org/10.5772/59153>
32. D. Sáez-rodríguez, J. L. C. Munoz, I. Johnson, D. J. Webb, and M. C. J, "Long period fiber gratings photo inscribed in a microstructured polymer optical fiber by UV radiation," vol. 7357, pp. 1–8, 2009. <https://doi.org/10.1117/12.823292>
33. Diez, T. a Birks, W. H. Reeves, B. J. Mangan, and P. S. J. Russell, "Excitation of cladding modes in photonic crystal fibers by flexural acoustic waves," *Optics Letters*, vol. 25, p. 1499 2000.

<https://doi.org/10.1364/OL.25.001499>

34. J. H. Lim, K. S. Lee, J. C. Kim, and B. H. Lee, "Tunable fiber gratings fabricated in photonic crystal fiber by use of mechanical pressure, " Optics Letters, vol. 29, pp. 331–333, 2004. <https://doi.org/10.1364/OL.29.000331>
35. D.D. Davis, T.K. Gaylord, E.N. Glytis, S.G. Kosinski, S.C. Mettler, and A.M. Vengsarkar "Long Period Fibre Grating Fabrication with Focused CO<sub>2</sub> Laser Pulses," Electronics Letters, vol. 34, no. 3, pp. 302-303, 1998. <https://doi.org/10.1049/el:19980239>
36. B.H. Kim, T. Ahn, D.Y. Kim, B.H. Lee, Y. Chung, U.C. Paek, and W.T. Han. "Effect of CO<sub>2</sub> laser irradiation on the refractive-index change in optical fibers," Applied Optics, vol. 41, no. 19, pp. 3809-3815, 2002. <https://doi.org/10.1364/AO.41.003809>
37. M. Akiyama, K. Nishide, K. Shima, A. Wada, and R.Yamauch. "A Novel Long-period Fiber Grating Using Periodically Releases Residual Stress of Pure-silica Core Fiber," Optical Fiber Communication Conference (OFC), vol. 2 pp. 276-277, 1998. <https://doi.org/10.1109/OFC.1998.657397>

38. Y. Wang, "Review of Long Period Fiber Gratings Written by CO<sub>2</sub> Laser," *Journal of Applied Physics*, vol. 108, no. 8, 2010. 081101<https://doi.org/10.1063/1.3493111>
39. H. Chan, E. Perez, F. Alhassen, I. Tomov, H. Lee, "Ultra-Compact Long-Period Fiber Grating and Grating Pair Fabrication using a Modulation-Scanned CO<sub>2</sub> Laser," *Conference on Optical Fiber Communication and the National Fiber Optic Engineers Conference*, pp. 1-3, 2007. <https://doi.org/10.1109/OFC.2007.4348437>
40. DC. Alves, J. Coelho, M. Nespereira, F. Monteiro, M. Abreu, J.M. Rebordão, "Automation methodology for the development of LPFG using CO<sub>2</sub> laser radiation," *Lasers, and Applications*, p. 6, 2013. <http://dx.doi.org/10.1117/12.2026249>
41. H.S. Ryu, Y.W. Park, S.T. Oh, Y.J. Chung, D.Y. Kim, "Effect of asymmetric stress relaxation on the polarization-dependent transmission characteristics of a CO<sub>2</sub> laser-written long-period fiber grating," *Optical Letters*, vol. 28, no. 3, pp. 155–157, 2003. <https://doi.org/10.1364/ol.28.000155>
42. Y.J Rao, T Zhu, Z.L Ran, Y.P Wang, J Jiang, A.Z Hu, "Novel long-

- period fiber gratings written by high-frequency CO<sub>2</sub> laser pulses and applications in optical fiber communication,” *Optics Communications*, Vol. 229, no. 1–6, pp. 209-221, 2004.  
<https://doi.org/10.1016/j.optcom.2003.10.048>
43. T. Zhu, K. S. Chiang, Y. J. Rao, C. H. Shi, Y. Song, and M. Liu, “Characterization of Long-Period Fiber Gratings Written by CO<sub>2</sub> Laser in Twisted Single-Mode Fibers,” in *Journal of Lightwave Technology*, vol. 27, no. 21, pp. 4863-4869, 2009. doi: 10.1109/JLT.2009.2029542.
44. R.B. Shang, “Fabrication of twisted long-period fiber gratings with high-frequency CO<sub>2</sub> laser pulses and its bend sensing,” *Journal of Optics*, vol. 15 no. 7, p. 5402, 2013. <httpS://doi.org/10.1088/2040-8978/15/7/075402>
45. Y.P. Wang and D.N. Wang, “Asymmetric long period fiber gratings fabricated by use of CO laser to carve periodic grooves on the optical fiber,” *Applied physics letters*, vol. 89, no. 15, 2006.  
<http://dx.doi.org/10.1063/1.2360253>
46. L. Su, K.S. Chiang, and C. Lu, “CO<sub>2</sub> laser-induced long-period

- gratings in graded-index multimode fibers for sensor applications,”  
IEEE Photonics Technology Letters, vol. 18, no. 1, pp. 190–192, 2006.  
<https://doi.org/10.1109/LPT.2005.861267>
47. C.S. Kim, Y. Han, B.H. Lee, W.T. Han, U.C. Paek, Y. Chung,  
“Induction of the refractive index changes in B-doped optical fibers  
through relaxation of the mechanical stress,” Optics Communications,  
vol. 185, no. 4-6, pp. 337-342, 2000. [https://doi.org/10.1016/S0030-4018\(00\)01045-2](https://doi.org/10.1016/S0030-4018(00)01045-2)
48. B.H. Kim, Y. Park, T.J. Ahn, B.H. Lee, Y. Chung, U.C. Paek, W.T.  
Han, “Residual stress relaxation in the core of the optical fiber by CO2  
laser radiation”. Optical Letters, vol. 26, no. 21, pp. 1657-1659, 2001.  
<https://doi.org/10.1364/OL.26.001657>
49. G. Kakarantzas, T.A. Birks, P.S. Russell, “Structural long-period  
gratings in photonic crystal fibers”. Optical Letters, vol. 27, no. 12,  
pp. 1013–1015, 2002. <https://doi.org/10.1364/OL.27.001013>
50. Y. Liu, K.S. Chiang, “Recent development on CO2 laser written long-  
period fiber gratings”, Passive Components and Fiber-based Devices,  
Proceedings of SPIE, pp. 713-437, 2008.



<https://doi.org/10.1117/12.802448>

51. J. Han, J. Kim, S.-L. Lee, S. Choi, and Y. W. Lee, “Simultaneous measurement of torsion and temperature based on  $\pi$ -phase-shi long-period fiber grating inscribed on double-clad fiber,” *Journal of Nanoscience and Nanotechnology*, vol. 21, no. 8, pp. 4243–4251, 2021. <https://doi.org/10.1166/jnn.2021.19403>
52. R. Ranjan, F. Esposito, S. Campopiano, and A. Iadicicco, “Sensing characteristics of arc-induced long-period gratings in polarization-maintaining panda fiber, ” *IEEE Sensors Journal*, vol. 17, no. 21, pp. 6953–6959. 2017. <https://doi.org/10.1109/JSEN.2017.2755370>
53. X. He, J. Zhou, L. Meng, K. Zhang, X. Wang, S. Zhang, W. Li, and L. Yuan, “Directional torsion sensor based on long-period fiber gratings inscribed by a periodically micro taper,” *Optical Fiber Technology*, no. 71, p. 102908, 2022. <https://doi.org/10.1016/j.yofte.2022.102908>

## **Acknowledgments**

In the name of Allah, the Most Gracious and the Most Merciful

All praise to Allah and his blessing for the completion of this thesis. Our humblest gratitude to the Rasulullah Muhammad PBUH whose way of life has been a continuous guidance for us. Furthermore, to my parents, who always pray and encourage me to live a good life.

I also would like to sincerely thank to my Professor Yong Wook Lee for allowing me to study, explore, and innovate in the laser-based optical application lab, as well as providing me with guidance, support, and inspiration through his disciplined, advanced, and creative thinking. I'd would like to take this occasion to express my gratitude to all the professors in the Department of Industry 4.0 Convergence Bionics Engineering and Brain Korea (BK21) program for the support while studies in Korea.

I'm also grateful to my LOA lab members including Jinsil Han, Minchan Bae, Jihoon Kim, Sungwook Choi, and Gangmin Bae who supported me in my research for creating a pleasant and comfortable working atmosphere. In addition, special thanks to my beloved wife Siti Aisyah Nurmaulia Entifar and my daughter Hanna Shafiya Yasira Syahnata who always help and accompany me in difficult and happy situations in South

Korea, who motivate me to achieve every success I have in my life

Busan, February 2022

Jonatan Martino Windi Saputro

